Turbulence in superfluid helium: Steady homogeneous counterflow

K. W. Schwarz
IBM Thomas J. Watson Research Center, Yorktown Heights, New York 10598
(Received 9 December 1977)

The fully developed turbulent state of a superfluid is considered in the simple limit of homogeneous counterflow. The vortex tangle is described in statistical terms which focus on the distribution of line length with respect to the local self-induced velocity v_l of the line. The equation for the motion of a line element is found to contain driving terms arising from the interaction of the normal fluid with the line element, and randomizing terms arising from its self-induced motion. A geometrical argument indicates that a random tangle has a characteristic distance over which all local derivatives randomize. A dynamical argument suggests that line-line crossings lead to a characteristic randomization distance equal to the typical interline spacing δ, and to a characteristic randomization time of order $\delta/\langle v_l \rangle$. Setting the geometric randomization distance equal to δ then allows one to model the effect of the self-induced motion as a kind of random walk. The resulting complicated differential equation predicts steady-state properties in good agreement with those observed experimentally. It is also found that the well-known Vinen equation follows as an accurate consequence of the theory. The physical interpretation of this equation, however, turns out to be different from that which was originally proposed.

I. INTRODUCTION

The flow of superfluid helium in channels of various geometries has been investigated in an enormous number of experiments. These range from studies of unsaturated helium films, where the characteristic channel diameter d approaches a few angstroms and only the superfluid component can move, to the kind of experiment of particular interest to us here where d lies in the range 10^{-3}–1 cm and both the normal and superfluid velocities can be large. The classic version of the wide-channel experiments is illustrated in Fig. 1. A steady heat input $\dot{Q}$ generates an excess of elementary excitations in the dead end, leading to a volume flow rate of normal fluid $\dot{Q}/\rho ST$ out through the channel. Here ρ is the total fluid density and S is the entropy per unit mass, carried entirely by the normal fluid. In order to conserve mass, the normal fluid motion must be balanced by a flow of superfluid $\rho_n\dot{Q}/\rho_s ST$ in through the channel, where ρ_n and ρ_s are the normal and superfluid densities, respectively. In this way, a steady-state counterflow is set up with an average normal fluid velocity $V_n = \dot{Q}/A\rho ST$ and an average superfluid velocity $V_s = -\rho_n\dot{Q}/A\rho_s\rho ST$, where A is the cross-sectional area of the channel and the positive direction is taken outward. Other wide-channel experiments in which only V_s is nonzero, or in which V_n and V_s are independently variable have also been reported, but those done in the simple counterflow geometry have been the most extensive and seem to give the least ambiguous results.

A flow such as that shown in Fig. 1 will generate observable temperature and pressure differences between the two ends of the channel, with the characteristic behavior shown in Fig. 2. At low velocities both ΔT and ΔP exhibit a linear dependence that can be quantitatively understood from the usual two-fluid equations by assuming the laminar flow of both the normal and superfluid components through the channel.[1] As the flow is increased to some critical value, a new regime appears which is characterized primarily by a rapid nonlinear increase in ΔT, although careful measurements also show small systematic variations in ΔP. The onset of this extra dissipation arises from the instability of the laminar two-fluid motion against the appearance and growth of quantized vortices in the superfluid. The velocity field near the core of a quantized vortex varies rapidly over distances comparable to the wavelengths of the ambient elementary excitations and it will scatter these strongly. Thus, the generation of quantized vortices provides a mechanism for the dissipative interaction of the normal and the superfluid components of the motion.

The breakdown of laminar flow seems to be de-

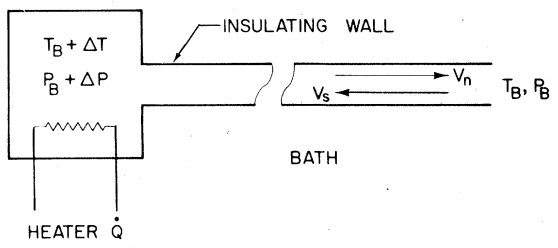

FIG. 1. Schematic of a typical counterflow experiment. The measured quantities are ΔT and ΔP.

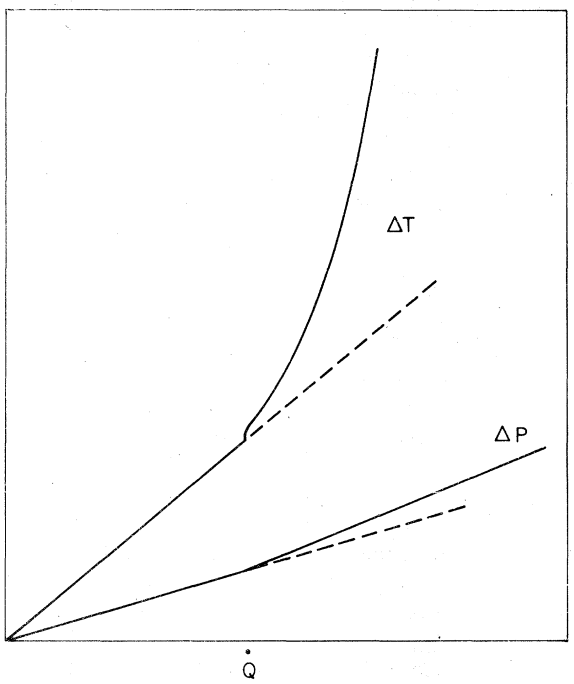

FIG. 2. Typical qualitative behavior of ΔT and ΔP, in arbitrary units.

termined, first, by the mechanisms available for generating vortex-line perturbations in the laminar flow field and, second, by the conditions under which such perturbations, once they are present, can grow because of their nonconservative interaction with the normal fluid and the walls of the channel. The interplay of these two factors leads to a very complicated phenomenology for the onset of dissipation, with at least two well-defined types of possible behavior. In sufficiently narrow channels the controlling element appears to be the rate at which microscopic vortex fluctuations of a critical size are thermally nucleated in the fluid. Each such fluctuation is assumed to grow and annihilate at the walls of the channel, resulting in a well-defined amount of energy exchanged between the superfluid and the thermal reservoir. In this *intrinsic* regime,[2] the onset of dissipation is found to exhibit a number of regular and repeatable features consistent with the idea of a thermally activated relaxation process. In wide channels, however, one observes a distinctly different *extrinsic* behavior, which is qualitatively similar to the onset of turbulence in a classical fluid, and which is strongly influenced by geometrical effects as well as ambient noise levels. In this regime, the dissipation at onset is often observed to switch on and off intermittently and to show hysteresis in a manner suggesting that vortex lines are randomly initiated by end effects or vibrations, and then grow or decay in some irregular way which depends on the detailed dynamical interaction of the line with the walls of the channel and the elementary excitations. Beyond the onset region, the dissipation becomes well defined, presumably because any vortex-line perturbation will grow into a random self-perpetuating vortex tangle filling the whole channel and possessing well-defined average properties.

It seems to be rather difficult to interpret the complicated properties of the onset region, but the fully developed turbulence achieved as the flow rates are increased should be more amenable to theoretical analysis. As the amount of vorticity in the fluid increases, the microscopic vortex tangle grows denser and the characteristic interline spacing δ becomes smaller. When δ becomes much smaller than the typical dimensions of the channel, the dynamics of the vortex tangle at a given point in the channel is presumably determined by its local properties and not by the geometry of the channel. Similarly, the random vorticity sources which are important in producing the intermittent behavior characteristic of the onset regime should become irrelevant when vorticity is constantly being created and destroyed everywhere by the hydrodynamic interaction between the normal fluid and the vortex tangle.

Indeed, there is considerable evidence that the fully developed turbulent state has some remarkably simple and general features. The most generally recognized of these was indicated by the early[3] observation that in the turbulent regime the excess temperature gradient along the channel in experiments of the type shown in Fig. 1 is simply proportional to $\dot{Q}^3$. From a phenomenological point of view, one can derive such temperature gradients by adding a *mutual friction force*[4] acting between the normal and superfluid components to the usual two-fluid equations describing laminar flow. This force density takes the form

$$\vec{F}_{sn} = -A(T)\rho_s\rho_n(V_{ns} - v_0)^2\vec{V}_{ns}\,, \tag{1}$$

where $\vec{V}_{ns} = \vec{V}_n - \vec{V}_s$, $A(T)$ is an experimentally determined function of temperature, and v_0 is a small, adjustable parameter of order 1 cm sec^{-1}. In a beautiful experiment wherein he measured the attenuation of a small and rapidly varying second-sound field $\vec{v}_{ns}$ by the turbulence, Vinen[5] found a frictional force density

$$\vec{F}'_{sn} = -A'(T)\rho_s\rho_n(V_{ns} - v_0)^2\vec{v}_{ns}\,. \tag{2}$$

As noted above, $\vec{F}_{sn}$ arises from the scattering of the elementary excitations, which compose the normal fluid, by the dense mass of quantized vortex lines characterizing the turbulent state. Since this force must be a linear function of the small

perturbing field $\vec{v}_{ns}$, Vinen concluded that the observed relationship (2) implies that the steady-state density of the vortex tangle has the dependence

$$L = a(T)(V_{ns} - v_0)^2 , \tag{3}$$

where L denotes the line length per unit volume, and $a(T)$ can be determined from the experimental function $A'(T)$. In this early work it was assumed that A' and A are the same. However, since the vortex tangle is not in general isotropic, the relationship between A and A' is somewhat more complicated, and (1) and (3) in principle provide different kinds of information.[6]

Because the temperature gradients observed experimentally are rather large, the usefulness of the mutual friction idea has long been established. Somewhat more controversial has been the concept of an additional effective force $\vec{F}_s$, acting on the superfluid alone, which may arise from an "eddy viscosity" associated with the motion of the vortex tangle. Brewer and Edwards[7] did observe that the onset of turbulence led to small excess differences $\Delta P'$, which could be ascribed to the existence of such a force. The more recent measurements of Childers and Tough,[8] although limited to narrow channels, show that this excess pressure drop also seems to have a rather simple variation, something like

$$\Delta P' \propto (V_{ns} - v_0)^{7/3} . \tag{4}$$

That this dissipative contribution should indeed be discussed in terms of a superfluid eddy viscosity is, however, by no means established.

In addition to those experiments in which the temperature and pressure differences between the two ends of a channel are measured, there have been several ingenious attempts to gain more detailed insights into the nature of the superfluid turbulent state. We have already mentioned the work of Vinen using second sound to detect the vortex tangle. This technique is currently being applied by Moss and co-workers[9] to investigate fluctuations in the vortex-line density. Another technique uses externally injected ions. Although it raises certain additional difficulties of interpretation, it has perhaps the greatest potential. Ions are trapped and released by the core of a quantized vortex in a reasonably well-understood way, and they can in principle be used to probe the local structure of the turbulent state. So far, several interesting insights have been obtained by means of these probes. The initial study[10] of the attenuation of an ion current as it passes through the turbulence provided striking additional evidence for the physical picture of a dense vortex tangle permeating the superfluid. Further measurements along these lines[11] have lent detailed support to the experimental relationship expressed by Eq. (3). Perhaps more interesting is the discovery of Ashton and Northby[12] that in simple counterflow the vortex tangle as a whole has an average drift velocity $\langle \vec{v}_l \rangle$ with respect to the superfluid rest frame. Again, this quantity appears to obey a simple law

$$\langle \vec{v}_l \rangle = b(T)\vec{V}_{ns} . \tag{5}$$

The existence of $\langle \vec{v}_l \rangle \neq 0$ is of importance in demonstrating that the vortex tangle is not isotropic in its properties. While such a result is not surprising given the anisotropic nature of the counterflow which drives the turbulence, previous discussions had always assumed an isotropic vortex tangle.

It is important to realize that relationships (1)–(5) have at present only a very approximate significance. All of the experiments discussed above have been interpreted by assuming that the local driving velocities in the channel are the *average* flow velocities V_n and V_s, and that the derived quantities $\vec{F}_{sn}$, $\vec{F}_s$, L, and $\langle v_l \rangle$ are constant throughout the channel. This, of course, is a gross simplification. In actual fact, the normal fluid velocity must vary from a maximum value of order V_n at the center of the channel to zero at the walls, and a realistic analysis should allow for a corresponding variation in the local properties of the vortex tangle. Thus, while various experimenters have claimed to measure accurate values of, e.g., $\vec{F}_{sn}$ and L, such values can be meaningful only in a semiquantitative sense.

We here try to sum up what is a very complicated experimental situation. The functional relationship between F_{sn} and V_{ns} of Eq. (1) appears to be a well-established property of uniform vortex turbulence, having been observed by many investigators. The coefficient $A(T)$ derived from various experiments is given in Fig. 3. For counterflow experiments (solid curves), one sees a reasonably universal temperature dependence, but only approximate agreement in the magnitude of A. It is one of the features of the theory to be developed in this paper that F_{sn} is predicted to be a function of the relative velocity V_{ns} *only*, regardless of the actual values of $\vec{V}_n$ and $\vec{V}_s$. It is therefore most interesting to note (curve d) that a measurement[15] in which only $\vec{V}_n$ is allowed to be nonzero gives compatible results. An experiment[16] in which only $\vec{V}_s$ is nonzero (curve e) seems to give a somewhat different temperature dependence, but this appears to be contradicted by a later explicit finding by the same group[17] that F_{sn} is indeed a function of V_{ns} only. The properties represented by Eqs. (2)–(5) have only been observed in particular experiments. As we shall

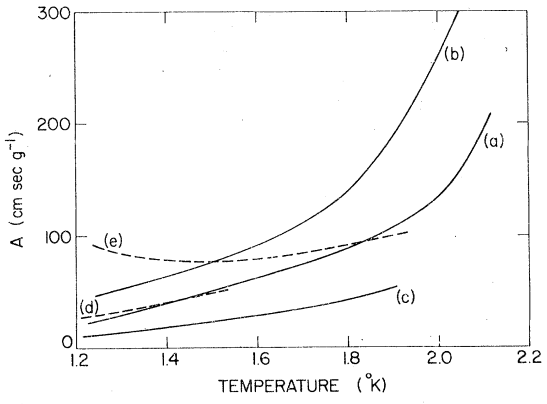

FIG. 3. Mutual friction coefficient observed under various conditions: (a) $d \sim 0.5$ cm, counterflow (Ref. 5); (b) $d \sim 0.01$ cm, counterflow (Ref. 13); (c) $d \sim 0.3$ cm, counterflow (Ref. 14); (d) $d \sim 0.03$ cm, pure normal fluid flow (Ref. 15); (e) $d \sim 0.03$ cm, pure superflow (Ref. 16).

see later, property (5) appears to have a physically straightforward interpretation in terms of the expected nonisotropic nature of the homogeneous turbulent state driven by uniform counterflow. The explanation of property (4), however, is unclear, particularly since $\Delta P'$ seems to arise from the inhomogeneous nature of channel flow. An experimenter setting up his own experiment is likely to observe features in addition to those already discussed. These can include the onset of turbulent flow in the normal fluid, the dependence of $A(T)$ on the nature of the channel walls, and various complicated geometry-dependent effects.

On the theoretical side, the most substantial contribution to our understanding of superfluid turbulence has been the early work of Vinen.[5] On the basis of a suggestion by Feynman[18] that the turbulent state consists of a tangled mass of quantized vortex lines, Vinen developed a phenomenological picture of a vortex tangle maintained in equilibrium by competing growth and annihilation processes. It was proposed, first, that the nonconservative interaction between the normal fluid and the vortex lines leads to a net vortex-generation term of the form

$$\left(\frac{dL}{dt}\right)_{\text{gen}} = \frac{\chi_1 B \rho_n}{2\rho} V_{ns} L^{3/2}, \tag{6}$$

where B is a known parameter describing the interaction between the line and the normal fluid, and χ_1 enters as an unkown function of temperature of order unity. Second, Vinen postulated a decay term

$$\left(\frac{dL}{dt}\right)_{\text{decay}} = -\frac{\chi_2 \kappa}{2\pi} L^2, \tag{7}$$

perhaps arising from line length lost through line-line collisions in the vortex tangle. Here χ_2 is another unknown temperature-dependent parameter of order unity, and κ is the quantum of circulation h/m_4. It is further proposed that the effect of the walls on the turbulence in the channel can be accounted for by simply assuming that the vortex generation mechanism is inactive within a characteristic distance from the wall for order $L^{-1/2}$. This is taken into account roughly by multiplying the vortex-generation term by a factor $(1 - \gamma/L^{1/2}d)$, with γ a parameter of order one. Thus the line density is supposed to be determined by the *Vinen equation*

$$\frac{dL}{dt} = \frac{\chi_1 B \rho_n}{2\rho} V_{ns} L^{3/2}\left(1 - \frac{\gamma}{L^{1/2}d}\right) - \frac{\chi_2 \kappa}{2\pi} L^2. \tag{8}$$

Given the freedom provided by its three adjustable functions χ_1, χ_2, and γ, Eq. (8) can be used to fit various experiments. First, it gives an equilibrium line density in agreement with Eq. (3). Second, it has been used to describe experiments on the transient behavior of vortex turbulence,[5] although the interpretation of these experiments in terms of homogeneous growth or decay mechanisms is open to question. Third, the work of Childers and Tough[8,19] has demonstrated the remarkable fact that Eq. (8) gives a reasonable description of the steady-state vortex line density in the region near the onset of turbulence, where δ becomes comparable to d and the model of a dense vortex tangle is not expected to hold at all. Finally, ion experiments[11] show that vortex lines release ions at a rate proportional to L^2, a result which has been interpreted in terms of a line-annihilation rate with the same dependence. While Vinen's equation has thus proved to be phenomenologically useful, its theoretical pedigree is obscure. The functional forms of the growth and annihilation terms in Eq. (8) have been supported only by dimensional arguments and an assumed analogy with classical turbulence. Not only is there no clear justification of Eq. (8), our subsequent discussion will in fact show that the dynamics of a vortex tangle is determined largely by effects that were ignored in Vinen's derivation, and that the physical interpretation of Eq. (8) must be radically modified.

As the preceding summary indicates, our understanding of superfluid turbulence is quite incomplete. A number of ingenious experiments have been devised to measure general properties of the turbulent state, but these continue to be interpreted in terms of a problematical phenomenology which represented a great step forward in its time, but which has neither been justified nor improved upon in the last twenty years. The work

presented here represents an effort to remedy this situation. We take the simplest physically relevant case, that of a vortex tangle in homogeneous counterflow, and develop a description consistent with the basic vortex-line dynamics. The predictions of the theory are then compared with those experimentally observed properties, represented by Eqs. (1), (3), and (5), which seem to characterize homogeneous counterflow. Although the derivation involves a number of gross simplifying approximations, the problem is complicated, and the resulting equation is still quite cumbersome. We therefore derive in Sec. V a reduced equation which turns out to be exactly of the form proposed by Vinen. A preliminary report of our work has been published previously.[20]

II. MOTION OF A VORTEX LINE

A vortex-line velocity field in the superfluid will change under the combined influence of the ideal fluid equations and of the nonconservative forces exerted near the core of the line by elementary excitations. We first consider the motion within the context of the ideal fluid equations which here take the form

$$\frac{\partial \vec{v}_s}{\partial t} + (\vec{v}_s \cdot \nabla)\vec{v}_s = -\frac{\nabla P}{\rho}, \tag{9}$$

$$\nabla \cdot \vec{v}_s = 0. \tag{10}$$

In addition, the superfluid velocity field $\vec{v}_s$ obeys the quantum restrictions

$$\nabla \times \vec{v}_s = 0, \tag{11}$$

$$\kappa \equiv \oint_L \vec{v}_s \cdot d\vec{l} = \frac{nh}{m_4}, \quad n = 0, 1, 2, \ldots, \tag{12}$$

where m_4 is the mass of the helium atom. To construct a quantized vortex one may simply draw a continuous curve, represented by the parametric form $\vec{s}(\xi, t_0)$, through the superfluid and require that the circulation κ about this line equal h/m_4. The solution of Eq. (11) subject to this boundary condition then consists of a macroscopic potential flow plus the field

$$\vec{v}_s(\vec{r}, t_0) = \frac{\kappa}{4\pi} \int_L \frac{(\vec{s} - \vec{r}) \times d\vec{s}}{|\vec{s} - \vec{r}|^3}, \tag{13}$$

where $\vec{r}$ is any point in the fluid. Equation (9) implies the Kelvin circulation theorem, which states that every point on the vortex line must move with the local fluid velocity. Thus the line moves according to the equation

$$\vec{v}(\xi_1, t) = \nabla\phi + \frac{\kappa}{4\pi} \int_L \frac{\vec{s}_{12} \times (\partial \vec{s}_{12}/\partial \xi_2)}{|\vec{s}_{12}|^3} d\xi_2, \tag{14}$$

where $\vec{s}_{12} = \vec{s}(\xi_2, t) - \vec{s}(\xi_1, t)$, and ϕ is the term arising from the macroscopic boundary conditions.

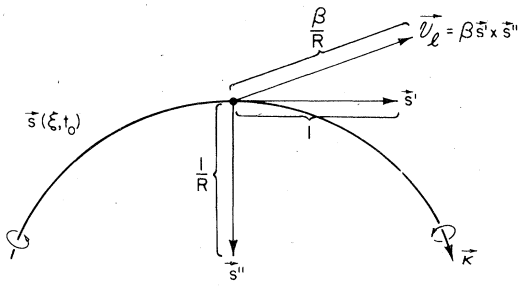

FIG. 4. Self-induced velocity of a curved vortex filament.

Although the prescription offered by Eq. (14) is straightforward, its nonlocal nature will make it an extremely tedious matter to calculate the time development of a complicated vortex configuration. An important simplification is obtained through the localized-induction approximation.[21,22] If in Eq. (14) the line is treated as an infinitely thin filament, the integral will diverge logarithmically as ξ_2 approaches ξ_1. The finite size of the core can be taken into account by introducing a suitable cutoff parameter a_0, confining the integration to $|\xi_2 - \xi_1||\partial \vec{s}/\partial \xi| \geq a_0$. It is also convenient to assume an outer limit of order $|\xi_2 - \xi_1||\partial \vec{s}/\partial \xi| \leq R$, where R is the local radius of curvature of the line. Then the local *self-induced velocity* at a point on the line is given by

$$\vec{v}_l(\xi, t) \approx \beta \frac{\partial \vec{s}/\partial \xi \times \partial^2 \vec{s}/\partial \xi^2}{|\partial \vec{s}/\partial \xi|^3}, \tag{15}$$

where $\beta = (\kappa/4\pi)\ln(R/a_0)$.[23] This neglects nonlocal terms of order $\kappa/2\pi\delta$, where δ is the characteristic interline distance to be discussed later. When ξ is taken to be the arc length, Eq. (15) simplifies to $\vec{v}_l = \beta \vec{s}' \times \vec{s}''$, primes denoting differentiations with respect to the arc length. The geometrical meaning of this relation is shown in Fig. 4. The relation $|\vec{s}''| = R^{-1}$ implies that the neglect of nonlocal terms gives rise to fractional errors in v_l of order $R[\delta \ln(R/a_0)]^{-1}$. Since a_0 is found experimentally to be about 10^{-4} cm, the localized induction approximation is accurate to about 10%.

We now discuss the effect of the force exerted by the normal fluid on the vortex core. A not-too-highly-curved vortex placed in the two-fluid velocity fields $\vec{v}_n$ and $\vec{v}_s$ experiences a force per unit length of the general form[24]

$$\vec{f} = [D(\vec{v}_n' - \vec{v}_s - \vec{v}_l - \vec{v}_{nc}) + D'\vec{s}'(\vec{v}_n' - \vec{v}_s - \vec{v}_l - \vec{v}_{nc})]_\perp, \tag{16}$$

where the $\perp$ indicates that only the components perpendicular to the line are to be considered. The quantity in parentheses is just the local average drift velocity of the excitation gas with re-

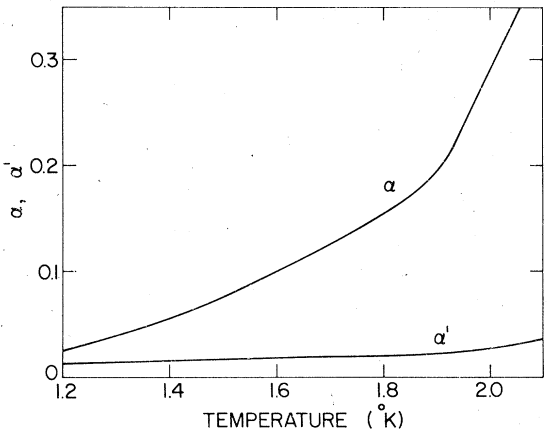

FIG. 5. Values of the mutual friction parameters used in our calculations.

spect to the vortex, which itself moves under the combined influence of the local average superfluid velocity $\vec{v}_s$, the self-induced velocity $\vec{v}_l$ of Eq. (15), and the velocity $\vec{v}_{nc}$ generated by the nonconservative force $\vec{f}$. In general, a distinction is drawn between $\vec{v}_n$ and the effective normal fluid velocity $\vec{v}_n'$ felt by the vortex core, since the presence of the vortex core can lead to a local dragging of the excitation gas.

The nonconservative motion $\vec{v}_{nc}$ of the vortex arises from the fact that the external force $\vec{f}$ acting on the core region must be passed on to the superfluid as a reaction force. For a rectilinear vortex this leads to

$$\vec{v}_{nc} = (\vec{s}' \times \vec{f})/\rho_s \kappa . \tag{17}$$

Equation (17) applies also to curved vortices[25] provided $R \gg a_0$. One may then insert Eq. (17) into Eq. (16) and solve for $\vec{v}_{nc}$:

$$\vec{v}_{nc} = \frac{\rho_n B_0}{2\rho} \vec{s}' \times (\vec{v}_n' - \vec{v}_s - \vec{v}_l) - \frac{\rho_n B_0'}{2\rho} \vec{s}' \times [\vec{s}' \times (\vec{v}_n' - \vec{v}_s - \vec{v}_l)] , \tag{18}$$

where

$$B_0 = (2\rho/\rho_n) D \rho_s \kappa / [D^2 + (\rho_s \kappa - D')^2] , \tag{19a}$$

$$B_0' = (2\rho/\rho_n)[D^2 - D'(\rho_s \kappa - D')]/[D^2 + (\rho_s \kappa - D')^2] . \tag{19b}$$

Substituting back into Eq. (16), one obtains for the force per unit length exerted on the vortex

$$\vec{f} = -\rho_s \kappa (\rho_n B_0/2\rho)\, \vec{s}' \times [\vec{s}' \times (\vec{v}_n' - \vec{v}_s - \vec{v}_l)] - \rho_s \kappa (\rho_n B_0'/2\rho)\, \vec{s}' \times (\vec{v}_n' - \vec{v}_s - \vec{v}_l) . \tag{20}$$

A bucket of helium rotating with an angular velocity Ω is filled with axially directed vortex lines distributed with a density $2\Omega/\kappa$ per cm^2. Thus, the average force exerted by the lines on the normal fluid is $-2\Omega \vec{f}/\kappa$, with $\vec{f}$ given by Eq. (20). This force can be determined by measuring the extra second-sound attenuation which is observed in rotating helium. Such experiments are customarily analyzed in terms of Eq. (20), with $\vec{v}_n'$ set equal to the local average $\vec{v}_n$, to yield phenomenological values of the mutual friction coefficients B, B'. Throughout the following discussion Eqs. (18) and (20) will be used in the same spirit, i.e., with B_0, B_0' set equal to the experimental coefficients B, B', and $\vec{v}_n'$ set equal to $\vec{v}_n$. This neglects the fact that roton-dragging corrections in a dense vortex tangle may differ from those appropriate to a rotating-bucket array. A similar approximation is involved in our assumption that these equations apply to vortex lines with characteristic radii of curvature of order 10^{-4} cm. The experimental values of $\alpha = \rho_n B/2\rho$ and $\alpha' = \rho_n B'/2\rho$ have been obtained from the paper by Lucas,[26] and are shown in Fig. 5.

III. DYNAMICS OF A VORTEX TANGLE

By the application of Eqs. (15) and (18) it is possible in principle to take a very complicated vortex configuration and to calculate how it will develop in time. Our much humbler aim is to find a simple approximate description of the vortex tangle which yet is sufficiently detailed to provide an explanation of the experimental observations discussed in Sec. I.

In order to avoid needless complications, one may suppose that the turbulence is driven by a constant and uniform counterflow velocity $\vec{V}_{ns}$, and that it is then possible to have a vortex tangle with spatially homogeneous properties. For the present we limit our considerations to this simple case (Fig. 6). The most basic feature of interest is then the length L of vortex line present per unit volume. A more detailed description could give

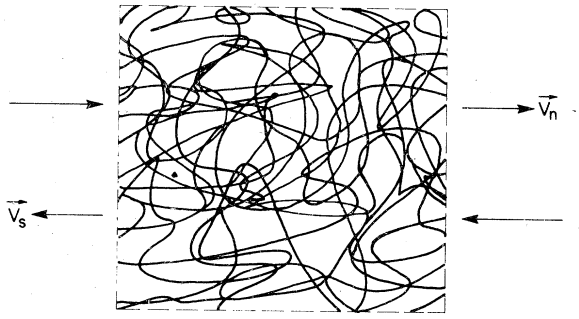

FIG. 6. Schematic rendering of a homogeneous vortex tangle subject to counterflowing normal and superfluid velocities.

the distribution of the line length with respect to some local properties of the line, such as the derivatives $\vec{s}'$, $\vec{s}''$, $\vec{s}'''$, ..., or some combination thereof. It is clear that the problem of describing such a random curve in greater and greater detail leads to mathematical considerations beyond the scope of our paper. On the other hand, if one works with a distribution involving only the first few derivatives, the question arises whether the specification of such a distribution at some particular time provides enough initial information to determine the subsequent development of the distribution. As we shall see, the answer is that it does not. Our method of dealing with this difficulty is to find a limited description of the tangle which is in sufficient harmony with the underlying behavior represented by Eqs. (15) and (18) that the dynamical effects of $\vec{s}'$ and $\vec{s}''$ are included in a natural way, and to obtain closure by treating the higher-order derivatives $\vec{s}'''$, $\vec{s}''''$, ... as random variables subject to certain physically reasonable restrictions.

Figure 5 shows that α' is rather small compared to α, and we therefore drop the corresponding terms in Eqs. (18) and (20). The basic equation of motion of the line then becomes

$$\vec{v} = \beta \vec{s}' \times \vec{s}'' + \alpha \vec{s}' \times (\vec{V}_{ns} - \beta \vec{s}' \times \vec{s}'') , \tag{21}$$

where, again, a prime denotes differentiation with respect to the arc length. It is apparent that the instantaneous motion of a point on the line is determined entirely by $\vec{v}_l = \beta \vec{s}' \times \vec{s}''$. Thus, a limited description of the tangle might usefully be given in terms of a distribution function $\lambda'(\vec{v}_l, t)$. Although we assume this distribution to be homogeneous, the counterflow velocity $\vec{V}_{ns}$ defines a preferred axis, and one is clearly not justified in assuming that λ' is isotropic. We do, however, limit our considerations to the azimuthally symmetric case $\lambda' = \lambda'(|\vec{v}_l|, \theta, t)$, where θ is the angle that $\vec{v}_l$ makes with the polar axis defined by $\vec{V}_{ns}$. Since the local radius of curvature R is just $\beta/|\vec{v}_l|$, one can define an equivalent distribution $\lambda(R, \theta, t)$, such that $\lambda(R, \theta, t) 2\pi R^2 \sin\theta \, dR \, d\theta$ is equal to the line length per unit volume with local radius of curvature in the range R to $R + dR$ and $\vec{v}_l$ heading into the cone between θ and $\theta + d\theta$. This will prove the more convenient.

For certain purposes, such as the evaluation of the mutual friction force, it will be necessary to consider the question of how the line length is distributed with respect to $\vec{s}'$ and $\vec{s}''$, rather than $\vec{v}_l$. We recall (Fig. 4) that $\vec{s}'$, $\vec{s}''$, $\vec{v}_l$ make up an orthogonal set of vectors with magnitudes, 1, $1/R$, β/R, respectively. For a given $\vec{v}_l$, one may choose an arbitrary $\vec{s}'$ perpendicular to $\vec{v}_l$, $\vec{s}''$ then being determined. In principle, this freedom in choosing $\vec{s}'$ allows one to construct a variety of distributions over $\vec{s}'$ and $\vec{s}''$ for a given λ, provided one is willing to permit the $\vec{s}'$ associated with a given $\vec{v}_l$ to be distributed nonsymmetrically about the axis defined by $\vec{v}_l$. Such an artifical distribution of $\vec{s}'$ is of course not required by our information about $\vec{v}_l$ and would in fact correspond to a very peculiar arrangement of the vorticity, such as might be present near a boundary. For homogeneous turbulence far from boundaries it is reasonable to take the line elements associated with a given $\vec{v}_l$ to be pointing with equal probability in all directions perpendicular to $\vec{v}_l$.

Let us now consider what happens to a line element of length Δl, every point of which is in motion according to Eq. (21). Since our description of the tangle keeps track of how much line there is and how it is distributed with respect to $\vec{v}_l$, it will be of particular interest to determine how Δl and $\vec{v}_l$ are changing. The nonconservative term can stretch or shrink the line, and it is temporarily convenient to specify a point on and moving with the line by a parameter ξ defined so as to be independent of time, rather than by the arc length. Then

$$\frac{\partial \vec{s}}{\partial t} = \vec{v}, \quad \frac{\partial}{\partial t}\frac{\partial \vec{s}}{\partial \xi} = \frac{\partial \vec{v}}{\partial \xi}, \quad \frac{\partial}{\partial t}\frac{\partial^2 \vec{s}}{\partial \xi^2} = \frac{\partial^2 \vec{v}}{\partial \xi^2}, \text{ etc.} \tag{22}$$

From these relations one computes other local properties of interest by use of the chain rule, e.g.,

$$\frac{\partial}{\partial t}\left|\frac{\partial \vec{s}}{\partial \xi}\right| = \frac{\partial \vec{s}/\partial \xi}{|\partial \vec{s}/\partial \xi|} \cdot \frac{\partial \vec{v}}{\partial \xi}, \tag{23}$$

$$\frac{\partial}{\partial t}\frac{\partial \vec{s}/\partial \xi}{|\partial \vec{s}/\partial \xi|} = \frac{\partial \vec{v}/\partial \xi}{|\partial \vec{s}/\partial \xi|} - \frac{\partial \vec{s}}{\partial \xi}\frac{(\partial \vec{s}/\partial \xi)\cdot(\partial \vec{v}/\partial \xi)}{|\partial \vec{s}/\partial \xi|^3}, \tag{24}$$

$$\frac{\partial}{\partial t}\frac{\partial^2 \vec{s}/\partial \xi^2}{|\partial \vec{s}/\partial \xi|^2} = \frac{\partial^2 \vec{v}/\partial \xi^2}{|\partial \vec{s}/\partial \xi|^2} - 2\frac{\partial^2 \vec{s}}{\partial \xi^2}\frac{(\partial \vec{s}/\partial \xi)\cdot(\partial \vec{v}/\partial \xi)}{|\partial \vec{s}/\partial \xi|^4}. \tag{25}$$

Since $\Delta l = \left|\partial \vec{s}/\partial \xi\right| \Delta \xi$, Eq. (23) determines the rate at which Δl changes. Equations (24) and (25) can be applied to Eq. (15) to determine the time rate of change of $\vec{v}_l$. The resulting equations, with ξ again set equal to the arc length parameter, are

$$\frac{\partial}{\partial t}\Delta l = \vec{s}' \cdot \vec{v}' \, \Delta l , \tag{26}$$

$$\frac{\partial}{\partial t}\vec{v}_l = \beta[\vec{s}' \times \vec{v}'' + \vec{v}' \times \vec{s}'' - 3\vec{s}' \times \vec{s}''(\vec{s}' \cdot \vec{v})] . \tag{27}$$

Here the time derivatives are to be interpreted as the rates of change observed for a particular element as we follow its motion, and the arc length derivatives are to be evaluated from the instantaneous configuration of the line. Insertion of the $\vec{v}$ given by Eq. (21) into these expressions leads, after considerable algebraic manipulations, to

$$\frac{1}{\Delta l}\frac{\partial \Delta l}{\partial t}=\frac{\alpha}{\beta}\vec{v}_l\cdot(\vec{V}_{ns}-\vec{v}_l)\,, \tag{28}$$

$$\begin{aligned}\frac{\partial}{\partial t}\vec{v}_l=&-\frac{\alpha}{\beta}\vec{v}_l\vec{v}_l\cdot(\vec{V}_{ns}-\vec{v}_l)-\frac{\alpha}{\beta}\vec{v}_l\times(\vec{v}_l\times\vec{V}_{ns})\\&+\beta^2[(\vec{s}'\times\vec{s}'')\times\vec{s}'''+\vec{s}'\times(\vec{s}'\times\vec{s}'''')]\\&-\alpha\beta\vec{s}'\times(\vec{s}'\times\vec{s}''')\vec{s}'\cdot\vec{V}_{ns}+2\alpha\beta^2\vec{s}'\vec{s}'\cdot(\vec{s}''\times\vec{s}''')\\&-\alpha\beta^2\vec{s}''\times\vec{s}'''-\alpha\beta^2\vec{s}'\times\vec{s}''''\,.\end{aligned} \tag{29}$$

One can distinguish between two kinds of terms in these equations. The term governing $\partial\Delta l/\partial t$, and the first two terms governing $\partial\vec{v}_l/\partial t$ depend only on the known quantities Δl and $\vec{v}_l$ themselves. These *driving terms*, taken by themselves, would cause the distribution λ to develop in a smooth nonrandom manner. The remaining terms in Eq. (29) are not only extremely complicated in their effect, but they depend on the higher-order local derivatives $\vec{s}'''$ and $\vec{s}''''$, which in themselves are not known within the context of these equations. It is nevertheless clear that in the case of a randomly winding line those elements of the line having a particular value of $\vec{v}_l$ can still have a variety of possible values of $\vec{s}'$, $\vec{s}''$, $\vec{s}'''$, $\vec{s}''''$. The higher order terms in Eq. (29) will therefore cause this group of line elements to disperse in $\vec{v}_l$ space.

Some simplification can be achieved by noting that $\alpha \ll 1$ at all temperatures except those very near the λ point. Equation (29) is therefore well approximated by

$$\begin{aligned}\frac{\partial}{\partial t}\vec{v}_l\approx&-\frac{\alpha}{\beta}\vec{v}_l\vec{v}_l\cdot(\vec{V}_{ns}-\vec{v}_l)-\frac{\alpha}{\beta}\vec{v}_l\times(\vec{v}_l\times\vec{V}_{ns})\\&+\beta^2[(\vec{s}'\times\vec{s}'')\times\vec{s}'''+\vec{s}'\times(\vec{s}'\times\vec{s}'''')]\,,\end{aligned} \tag{29'}$$

which contains only the dominant higher-order term, arising from the self-induced motion of the line. The qualitative picture which emerges then is that each part of the distribution λ is driven to move in a well-defined direction in $\vec{v}_l$ space by the interaction between the normal fluid and the vortex tangle. Competing with this there is a tendency for each part of λ to spread out in all directions, arising primarily from the complicated self-induced motions that exist within a random tangle.

A. Driving terms

It is easy to show that the driving terms lead to the simple relations

$$\frac{1}{\Delta l}\frac{\partial}{\partial t}\Delta l=\frac{\alpha}{R}(V_{ns}\cos\theta-\beta/R)\,, \tag{30}$$

$$\frac{\partial R}{\partial t}=\alpha(V_{ns}\cos\theta-\beta/R)\,, \tag{31}$$

$$\frac{\partial\theta}{\partial t}=-\alpha V_{ns}\sin\theta/R\,. \tag{32}$$

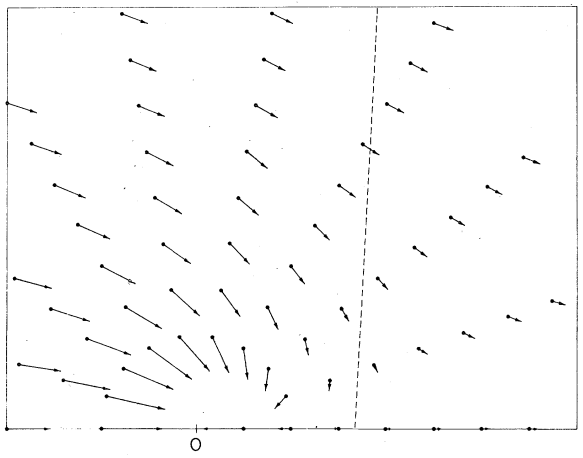

FIG. 7. Flow field $\dot{R}\hat{R}+R\dot{\theta}\hat{\theta}$ generated by the nonconservative forces, in arbitrary units. The figure corresponds to $V_{ns}=10$ cm sec^{-1}. Points are spaced 10^{-4} cm apart in the radial direction, and 20° apart in angle. $\vec{V}_{ns}$ points from left to right, and the line-growth region lies to the right of the dashed line.

A given line element will increase in length if the component of V_{ns} in the direction of $\vec{v}_l$ is greater than $|\vec{v}_l|=\beta/R$, i.e., if the normal fluid is "pushing" the line element from behind. This growth is accompanied by an increase in R. Line elements for which $(V_{ns}\cos\theta-\beta/R)<0$, on the other hand, will shrink and decrease in R. In addition, the angular term (32) rotates $\vec{v}_l$ into the forward direction. The effect of these factors on the distribution is indicated schematically in Fig. 7. It is apparent that λ is constantly gaining line length in a region where $\vec{v}_l$ points in the forward (small θ) direction, and is losing it elsewhere. It follows that the driving terms can lead either to a net growth or decay of the total line length, depending on how λ is distributed, but that they are always working to polarize the vortex tangle so that $\vec{v}_l$ points preferentially in the direction of $\vec{V}_{ns}$.

To express the effect of the driving terms on λ analytically, consider what happens during a time interval dt to the line length $\lambda(R,\theta,l)d^3w$ initially contained in a particular volume element d^3w of R, θ space. The values of R, θ associated with this particular collection of line elements will change according to Eqs. (31) and (32), the actual length of line will increase or decrease according to Eq. (30), and the volume element d^3w will become distorted to a new shape $d^3w(t+dt)$. Hence, we have

$$\begin{aligned}&\lambda(R+\dot{R}dt,\,\theta+\dot{\theta}\,dt,\,t+dt)d^3w(t+dt)\\&\qquad=\left(1+\frac{\Delta\dot{l}\,dt}{\Delta l}\right)\lambda(R,\theta,t)d^3w(t)\,.\end{aligned} \tag{33}$$

The change in d^3w may be calculated by thinking

of $\dot{R}dt$, $\dot{\theta}dt$ as a displacement field $\vec{q}(r, \theta)$ in R, θ space and using the result $d^3w' = (1 + \nabla \cdot \vec{q}) d^3w$ familiar from the theory of elasticity. The result is

$$d^3w(t+dt) = [1 - (\alpha\beta/R^2)dt] d^3w(t) . \tag{34}$$

It is now a simple matter to expand Eq. (33) to first order in dt, and to insert Eqs. (30) to (32). One finds that the nonconservative driving terms generate a contribution

$$\dot{\lambda}_{nc} = \alpha\left(\frac{\beta}{R} - V_{ns}\cos\theta\right)\frac{\partial\lambda}{\partial R} + \alpha V_{ns}\frac{\sin\theta}{R}\frac{\partial\lambda}{\partial\theta} + \alpha V_{ns}\frac{\cos\theta}{R}\lambda . \tag{35}$$

B. Higher-order terms

It is apparent from Fig. 7 that the driving terms alone do not lead to a physically reasonable state. Any initial distribution with nonzero values in the forward region will grow without limit, while continuously moving to larger R and smaller θ. The idea now is that by including the higher-order terms in Eq. (29′) one may hope to generate additional contributions to $\partial\lambda/\partial t$ which limit this runaway behavior.

It has already been argued that the qualitative effect of the higher-order terms is to cause a kind of diffusion of λ in $\vec{v}_l$ space. Since, however, the description of the vortex tangle in terms of λ gives no information about $\vec{s}'''$ and $\vec{s}''''$, the development of a specific model for this process requires an extension of our arguments. To develop the discussion in an intuitively appealing manner, we consider various possibilities for the local structure of the tangle (Fig. 8). Since the normal fluid effects always tend to decrease the line length associated with regions of high curvature, it seems reasonable to suppose that the vortex tangle would tend to an open structure, such as shown in Figs. 8(a) and 8(b), rather than the highly kinked structure shown in Fig. 8(c). A useful way of visualizing some of the properties of such an open structure is in terms of the artificial configuration shown in Fig. 8(d). The total line length per unit volume here is $L = 3/\Delta^2$, which permits one to conclude that the characteristic interline distance in an open configuration is given by $\delta \sim L^{-1/2}$.[27] In this general sense, the configuration of Figs. 8(a) and 8(b) are similar, and in terms of the localized induction approximation alone the configuration of Fig. 8(a) could in fact persist unchanged. It is, however, clear that if such a configuration is allowed to develop in time it will quickly become more highly kinked through the action of nonlocal velocity fields and line-line crossings. Thus, a random open structure as in Fig. 8(b) appears to be the most reasonable candidate.

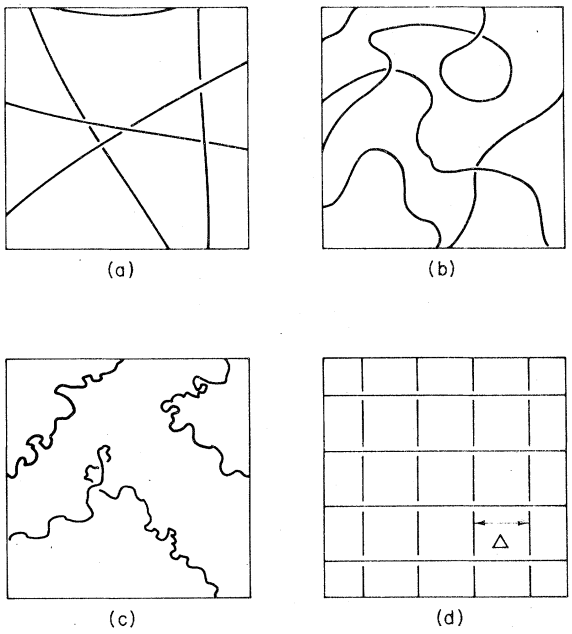

FIG. 8. Likely and unlikely candidates for the structure of the vortex tangle.

We now ask more specifically how the nonlocal effects neglected in the derivation of Eq. (15) act on the tangle. Because of the other lines in its vicinity, a given line segment is constantly subjected to random velocity fields of order $\kappa/2\pi\delta$. It will be shown later that these "long-range" fields are not a major factor. More important, the random motion of the line in Fig. 6 will lead to frequent line-line crossings. Computer simulations[28] of the motion of two closely approaching vortex lines show that during the crossing only very localized regions on the two lines are strongly distorted. These distortions then propagate relatively slowly along the lines. Such calculations cannot predict the eventual outcome of a crossing event but one reasonable set of possibilities is shown in Fig. 9. Whether this scenario is valid or not, the calculations imply that the qualitatively significant effect of the crossing is to generate large random disturbances at local points on the line, without causing major changes in L or the distribution of $\vec{v}_l$.

Consider a line element at some point A on the tangle. Its properties will be changing in a coherent way according to Eq. (29′) and the higher-order equations which can be derived from Eq. (15). However, its properties also will eventually be changed in a random way when a crossing event occurs at some other point on the line, and the

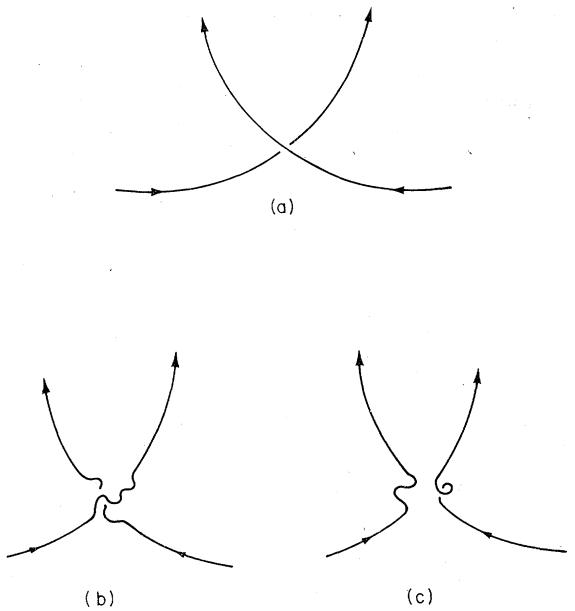

FIG. 9. One guess about what will happen when two vortex lines cross (a). They break and reconnect (b), or break and cross-connect (c).

"signal" from this event propagates to A. Now a random tangle such as shown in Fig. 8(b) will have a nonzero characteristic curvatures $\langle s''\rangle$, and therefore a representative line element will be moving through the tangle with a characteristic velocity $\langle v_l\rangle \sim \beta\langle s''\rangle$. The motion of the line through the tangle is shown schematically in Fig. 10. If the signal propagation velocity v_{sig} along the line is large, then the signal which randomizes A is likely to occur very quickly and to come from a line crossing very far from A; whereas if v_{sig} is small, the signal is likely to come from nearby and to take a long time to occur. *Thus, the existence of a finite* v_{sig} *means that there must be a characteristic time* τ *in which a typical line element becomes randomized by line-line crossing events, and that this randomization occurs over a characteristic length* $l = v_{sig}\tau$ *of the line.* More precisely, it may be seen by inspection of Fig. 10 that the probability of a crossing in the space and time intervals $(x, x+dx)$ and $(t, t+dt)$ is $(\langle v_l\rangle/\delta^2)\,dx\,dt$. If the line in Fig. 10 is assumed to be coherent at $t=0$, the probability of a signal arriving at A in $(t, t+dt)$ is then $(\langle v_l\rangle v_{sig} t/\delta^2)dt$. The probability that a signal has *not* arrived at A by the time t is $\exp(-\langle v_l\rangle v_{sig} t^2/2\delta^2)$, so that

$$\tau = \int_0^\infty t(\langle v_l\rangle v_{sig} t/\delta^2)\exp(-\langle v_l\rangle v_{sig} t^2/2\delta^2)dt\,. \tag{36}$$

Thus,

$$\tau \sim \delta/(\langle v_l\rangle v_{sig})^{1/2}\,,$$
$$l \sim \delta(\langle v_l\rangle/v_{sig})^{1/2}\,. \tag{37}$$

To estimate v_{sig} and to see how the existence of the characteristic randomization quantities τ, l enters into Eq. (29′) it is necessary to consider some general properties of the random tangle that we have not yet used. To begin, we note that $\vec{s}'$, $\vec{s}''$, $\vec{s}'''$, $\vec{s}''''$, ... are not entirely independent of one another. From the geometrical relation

$$\vec{s}'\cdot\vec{s}'' \equiv 0\,, \tag{38}$$

it is possible, by taking derivatives with respect to the arc length, to derive a series of constraints:

$$\vec{s}'\cdot\vec{s}''' + |\vec{s}''|^2 = 0\,,$$
$$3\vec{s}''\cdot\vec{s}''' + \vec{s}'\cdot\vec{s}'''' = 0, \ldots\,, \tag{39}$$

which apply at every point on the line. This implies that in a random tangle where $\vec{s}'''$, $\vec{s}''''$ are not expected to be strongly correlated with $\vec{s}'$, $\vec{s}''$ one has the order of magnitude relations

$$|\vec{s}'''| \sim \langle s''\rangle^2\,, \quad |\vec{s}''''| \sim \langle s''\rangle^3, \ldots\,, \tag{40}$$

where $\langle s''\rangle$ has been defined before as the average curvature in the vortex tangle. Equations (40) may be interpreted as indicating that the characteristic distance one must move along the line before $\vec{s}''$, $\vec{s}'''$, $\vec{s}''''$, ... become uncorrelated with their initial values is of order $\langle s''\rangle^{-1}$.

The effective velocity v_{sig} for the propagation of the large random distortions characteristic of the tangle down the line can now be derived in a very general way by considering the self-induced motion of the vortex. For the self-induced motion, the line length is conserved. Hence, one can take higher order iterations of Eq. (22) with ξ equal to the arc length and $\vec{v} = \beta\vec{s}'\times\vec{s}''$, to obtain a series of equations

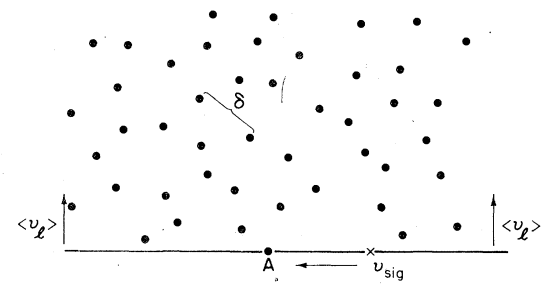

FIG. 10. Schematic of a line moving through the tangle. The dots represent places where the tangle intersects the plane of motion of the line.

$$\frac{\partial \vec{s}}{\partial t} = \beta \vec{s}' \times \vec{s}'', \quad \frac{\partial \vec{s}'}{\partial t} = \beta \vec{s}' \times \vec{s}''',$$

$$\frac{\partial \vec{s}''}{\partial t} = \beta(\vec{s}'' \times \vec{s}''' + \vec{s}' \times \vec{s}''''), \tag{41}$$

$$\frac{\partial \vec{s}'''}{\partial t} = \beta(2\vec{s}'' \times \vec{s}'''' + \vec{s}' \times \vec{s}''''')\,, \ldots,$$

describing the correlated, self-induced motion of the line. Locally the line will be curving as shown in Fig. 8(b), over a characteristic distance $\langle s'' \rangle^{-1}$, with values of $\vec{s}'''$, $\vec{s}''''$, ... of the typical magnitudes given by Eq. (40). This structure will undergo a complicated motion such that after some characteristic time the properties of the line at some point A will have changed by a large amount. Thus, for example, from the fourth of Eqs. (41) one can estimate the characteristic time in which $\vec{s}'''$ changes by an amount equal to its typical value:

$$\frac{\langle s'' \rangle^2}{\Delta t} \sim \beta(\langle s'' \rangle \langle s'' \rangle^3 + \langle s'' \rangle^4) \tag{42}$$

or

$$\Delta t \sim \frac{1}{\beta \langle s'' \rangle^2}. \tag{43}$$

Consideration of the higher-order equations shows that all derivatives change in the same characteristic time. In a general sense, this change represents the hydrodynamic propagation of the random deformation shown in Fig. 8(b) for a distance $\langle s'' \rangle^{-1}$ along the line, and in this sense

$$v_{sig} \sim \beta \langle s'' \rangle. \tag{44}$$

This, however, is just $\langle v_l \rangle$, so that Eq. (37) becomes

$$\tau \sim \delta / \langle v_l \rangle, \quad l \sim \delta. \tag{45}$$

To recapitulate, by considering the effect of line-line crossings within the tangle, we have found the elegant result that such events randomize the line over a characteristic distance of the order of the interline spacing, and that a given point on the line will become randomized in a characteristic time equal to the time it takes the line to move a distance of order δ through the tangle. *We now make the explicit assumption that the randomness of the tangle is maintained primarily by line-line crossings, in the sense that the characteristic distance one has to go along the line before* $\vec{s}''$, $\vec{s}'''$, ... *become uncorrelated with their initial values is assumed to be equal to* $l \sim \delta$. It is then intuitively plausible that

$$|\vec{s}'''| \sim \langle s'' \rangle / \delta, \quad |\vec{s}''''| \sim \langle s'' \rangle / \delta^2, \ldots, \tag{46}$$

These relations in fact follow from the geometrical requirements of Eq. (40), provided $\langle s'' \rangle \sim \delta^{-1}$. Since $\langle s'' \rangle$ can be evaluated from the distribution λ itself, it is not desirable to use this restriction explicitly. It will, however, be necessary to check that the model is self-consistent: the computed distributions should naturally exhibit the property $\langle s'' \rangle \sim L^{1/2}$. It is interesting to note that the structures of Figs. 8(a) and 8(c), which were rejected on intuitive grounds, correspond to $\langle s'' \rangle \ll L^{1/2}$ and $\langle s'' \rangle \gg L^{1/2}$, respectively, and hence do not satisfy this criterion, whereas that of Fig. 8(b) does.

Our physical model now is that line-line crossings keep the tangle random on a scale δ, implying that a given line element will have values of the higher-order derivatives which are randomly directed, but whose order of magnitude is restricted by Eq. (46). The line element will undergo correlated motion according to Eqs. (41), for a characteristic time $\tau \sim \delta / \beta \langle s'' \rangle$. It follows from the third order term in Eq. (29′) that during this time $\vec{v}_l$ will undergo a random rotation through an angle of order $\beta s''' \tau \sim 1$, while the fourth-order term generates a randomly directed displacement of the line element in $\vec{v}_l$ space of magnitude $\beta^2 s'''' \tau \sim \beta / \delta$. Since the line element plays for a new set of values $\vec{s}'''$, $\vec{s}''''$, ... after each τ, its motion is somewhat like a random walk, but one which involves large steps.

It may be noted at this point that, as stated earlier, the long-range velocity fields play an insignificant role. An element subject to a velocity field of order $\kappa / 2\pi\delta$ coming from a line a distance δ away will undergo a rate of change $\dot{s}'' \sim \kappa / 2\pi\delta^3$. This is to be compared with $\dot{s}'' \sim \beta \langle s'' \rangle^2 / \delta$, from Eqs. (41) and (46). With $\langle s'' \rangle \sim \delta^{-1}$ and β written explicitly, this becomes $\dot{s}'' \sim (\kappa / 4\pi\delta^3) \ln (R/a)$. Since the logarithm is of order 10, the self-induced motion dominates.

The random motion of the line elements obviously leads to a relaxation of λ, in competition with the effects of the nonconservative driving terms. For example, the angular motion generated by $\vec{s}'''$ implies that a λ peaked at some angle would spread out over an angular distance of order 1 in τ. In the heuristic spirit of the present discussion we model this in terms of a diffusive relaxation process. Since diffusion on the surface of a sphere of unit radius for a time t leads to an rms spread in angle equal to $(4Dt)^{1/2}$, we accordingly set $D = 1/4\tau$, and include a contribution

$$\dot{\lambda}_3 = \frac{\langle v_l \rangle}{4\delta} \left(\frac{\partial^2 \lambda}{\partial \theta^2} + \cot\theta \frac{\partial \lambda}{\partial \theta} \right). \tag{47}$$

The fourth-order term gives rise to a relaxation over a distance $\Delta = \beta / \delta$ in $\vec{v}_l$ space, in the characteristic time τ. For reasonably large v_l's, this corresponds to a distance $R^2 \Delta / \beta \sim R^2 / \delta$ in R space.

However, points near $\vec{v}_l = 0$, which on the average move to a much larger value of $\vec{v}_l$, relax over a distance of order R. A reasonable interpolation between these extremes is

$$\Delta R \sim R^2/(R+\delta)\,. \tag{48}$$

If this process is also to be modeled as a diffusive mechanism, the appropriate diffusion constant can then be determined from the three-dimensional formula $\langle \Delta R^2 \rangle \sim 6D\tau$. The resulting contribution to $\dot{\lambda}$ is then

$$\dot{\lambda}_{4,d} = \frac{\langle v_l \rangle}{6\delta}\left(\frac{R}{R+\delta}\right)^2 \left(R^2 \frac{\partial^2 \lambda}{\partial R^2} + 2R\frac{\partial \lambda}{\partial R} + \frac{\partial^2 \lambda}{\partial \theta^2} + \cot\theta \frac{\partial \lambda}{\partial \theta}\right). \tag{49}$$

One important factor which has been ignored in Eq. (49) is that an element with $v_l \sim \langle v_l \rangle$ undergoing a random step of order $\langle v_l \rangle$ is more likely to experience an increase in $|\vec{v}_l|$ than a decrease. If $\vec{v}_l' = \vec{v} + \beta \vec{a}/\delta$, where $\vec{a}$ is a random vector of order 1, then $v_l' \sim \langle (v_l^2 + 2\beta \vec{v}_l \cdot \vec{a}/\delta + \beta^2/\delta^2)^{1/2} \rangle \sim (\langle v_l \rangle^2 + \beta^2/\delta^2)^{1/2}$. Since $\beta/\delta \lesssim v_l$, this can be represented approximately as giving rise to a flux

$$\dot{R} \sim -\langle v_l \rangle R^2/\delta^2\,. \tag{50}$$

Equation (50) translates into an additional "kinking" contribution

$$\dot{\lambda}_{4,k} = \frac{\langle v_l \rangle}{\delta^2}\left(R^2 \frac{\partial \lambda}{\partial R} + 4R\lambda\right), \tag{51}$$

describing the fact that random changes in curvature are much more likely to kink up a straight line then they are to straighten out a highly curved one.

IV. CALCULATIONS

The equation describing the evolution of $\lambda(R, \theta, t)$ now becomes

$$\dot{\lambda} = \dot{\lambda}_{nc} + \dot{\lambda}_3 + \dot{\lambda}_{4,d} + \dot{\lambda}_{4,k}\,. \tag{52}$$

The characteristic self-induced velocity $\langle v_l \rangle$ and the interline distance $\delta = L^{-1/2}$ are to be evaluated self-consistently from λ. Thus, Eq. (52) contains no adjustable parameters whatever. It must be kept in mind, however, that our derivation has been based on order-of-magnitude arguments, and that we have modeled the randomization processes in a very crude and somewhat arbitrary manner. We now explore how well this approximate equation reproduces the experimental data discussed in Sec. I.

A. Method of integration

Equation (52) is difficult to integrate even numerically, and a survey of our procedure is appropriate here. In order to find the steady-state distribution corresponding to a given V_{ns} and temperature, we start with some artificial distribution and integrate Eq. (52), with the appropriate V_{ns} and $\alpha(T)$, forward in time. The equation is first converted to one in the dependent variable $u = \lambda R^2$ and the independent variables $z = \cos\theta$, $\xi = \ln R$. It is then written as a difference equation on a two-dimensional grid of equally spaced z, ξ values. The boundary conditions at $z = \pm 1$ arise naturally from the polar symmetry of the problem. However, there are no natural boundary conditions to be applied at the maximum and minimum values of ξ, and some additional arguments are required. At very small R, the dominant physical effect is that the nonconservative terms cause the line to decay rapidly to even smaller values of R, and all that matters is the convective $\partial\lambda/\partial R$ term in $\dot{\lambda}_{nc}$. However, this convective term is evaluated in our difference equation by referring to values of λ at larger R. It therefore turns out that the boundary condition at ξ_{min} has very little effect on the solution, and in practice $\partial u/\partial \xi$ is set to zero there. At very large R, on the other hand, the behavior is dominated by the convective kinking term $\dot{\lambda}_{4,k}$. If the distribution is zero for R larger than R_{max} it will never get large there. Thus u at ξ_{max} can also be set equal to zero. The validity of our procedure is indicated by the fact that if ξ_{min} is taken small enough and ξ_{max} large enough, the computed distribution becomes independent of these limits.[29]

As is usual with complicated equations of this type, an explicit forward integration of the resulting difference equation is unstable. The usual implicit methods, in which time-forward values are substituted for some of the terms in the difference equation and the resulting coupled system of equations is solved by a matrix diagonalization, proved much too time-consuming to be practical. A resolution of these difficulties was found in the use of the recently developed *hopscotch* algorithm,[30] which proved to be both stable and efficient. Another problem arises from the fact that, because of the variation of the self-induced velocity with R, those parts of λ which are at small R adjust themselves much more quickly that those at large R. The range of R included in the integration is large,[29] and a straightforward time integration requires very short steps in order to deal properly with the small-R region. For the purpose of finding the steady state solution, this difficulty can be overcome by using a time step adjusted to be a linear function of R. Equation (52) then still relaxes mathematically to the steady state $\partial\lambda/\partial t = 0$, but the manner in which it does so no longer represents the physical behavior of the system.

Figure 11 shows how the distribution relaxes from

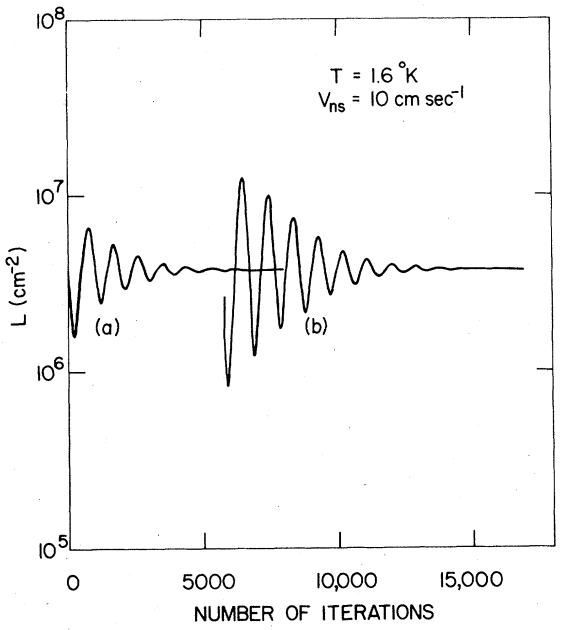

FIG. 11. Relaxation of λ to a steady state, according to Eq. (52). Starting conditions are (a) $\lambda R^2 \propto (1+\cos\theta)\delta(R-1.12\times10^{-4})$ with the proportionality constant adjusted so that $L = 3.4\times10^6$; (b) $\lambda R^2 =$ constant, with $L = 2.1\times10^7$. The beginning of curve (b) has been omitted.

various artificial initial states. The first point to note in favor of Eq. (52) is that λ does relax to a well-defined steady state, independent of the initial conditions. The peculiar oscillations seen in this figure are connected with the nonlinear nature of the equation: both $\langle v_l \rangle$ and $\delta = L^{-1/2}$ are evaluated as integrals over λ at each step of the integration. If, instead, one sets $\langle v_l \rangle = \beta \langle s'' \rangle = c\beta/\delta$, the convergence is much faster (Fig. 12). Thus, it is generally more efficient to let λ relax assuming various values of c, and then to pick that solution for which the computed $c = \langle v_l \rangle \delta/\beta$ equals the assumed c. It is at present not clear whether the transient oscillations of Fig. 11 or Fig. 12 are indicative of a real phenomenon or whether they represent some artifical feature of our equation or our method of solution.

B. Results

A typical steady-state solution of Eq. (52) is shown in Fig. 13. It is apparent that the predicted distributions are strongly polarized in the $\vec{V}_{ns}$ ($\theta = 0$) direction, and that they peak at a rather well-defined R. Once such a distribution has been calculated, the quantities F_{sn}, L, and $\langle v_{l2} \rangle$ can be computed as simple integrals over the distribution. Figures 14–16 show how these quan-

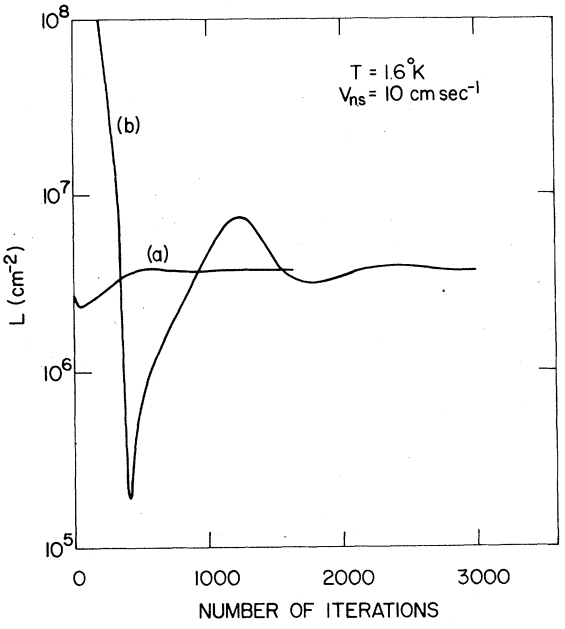

FIG. 12. Relaxation of λ when $\langle v_l \rangle$ is set equal to $c\beta/\delta$. The starting conditions are the same as those of Fig. 11.

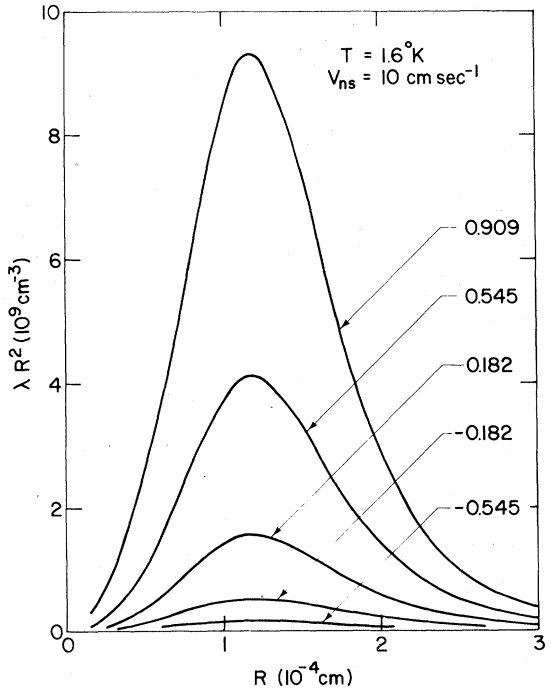

FIG. 13. Typical equilibrium distribution. Curves are given for various values of $\cos\theta$.

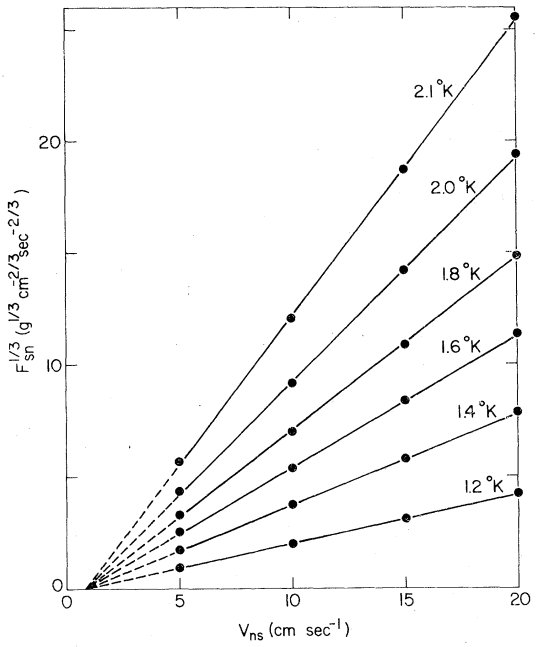

FIG. 14. Predicted behavior of the mutual friction F_{sn}. The dots are the values actually computed, the lines are the best straight-line fits. The experimental result [Eq. (1)] is that $F_{sn}^{1/3} \propto (V_{ns} - \frac{2}{3}v_0)$, to an accuracy $(v_0/V_{ns})^2$.

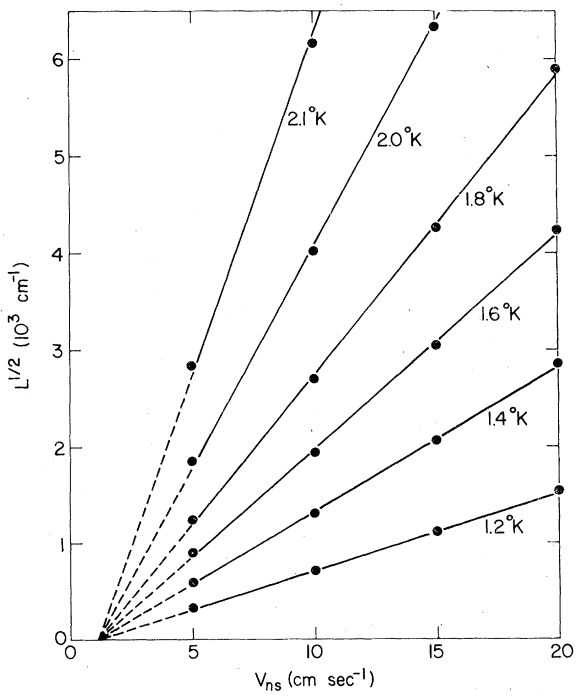

FIG. 15. Predicted behavior of the total line length density. The dots are the values actually computed, the lines are the best straight-line fits. The experimental result [Eq. (3)] is that $L^{1/2} \propto (V_{ns} - v_0)$.

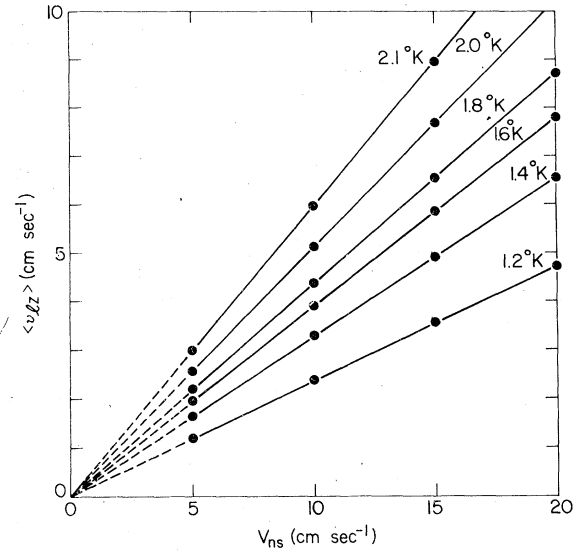

FIG. 16. Predicted behavior of the mean drift velocity of the tangle. The dots are the values actually computed, the lines are the best straight-line fits. The experimental result Eq. (15) is that $\langle v_{lz} \rangle \propto V_{ns}$.

tities depend on V_{ns}. The predicted behavior of all of these quantities is in remarkably good agreement with the experimental observations [Eqs. (1), (3), and (5)] at all temperatures. The theory predicts not only the observed power-law dependences, but also the existence and magnitude of the small parameters v_0. It is amusing to note further that a small deviation of F_{sn} above the cubic behavior has occasionally been observed, and our calculation seems to show an effect of this kind. Given the approximate nature of the theory, however, and the fact that significant approximations are made in the numerical analysis, it is probably wise at this stage not to place too much confidence in such detailed features.

From the straightline fits in Figs. 14–16 one can obtain $A(T)$, $\alpha(T)$, and $b(T)$. The computed values of these coefficients are compared with experiment in Figs. 17–19. In making the comparison it should be kept in mind that the experimental data are quite approximate, that the theory is expected to give only rough results, and that the predictions of the theory depend very sensitively on $\alpha(T)$, the effective behavior of which near the λ point is not well understood.[31] Nevertheless, there appears to be surprisingly good agreement, both in the magnitude and in the temperature dependence of the coefficients.

It is of interest to ascertain how dependent our predictions are on the details of the modeling used to develop Eq. (52). Considerable effort has been devoted to exploring this question. Our

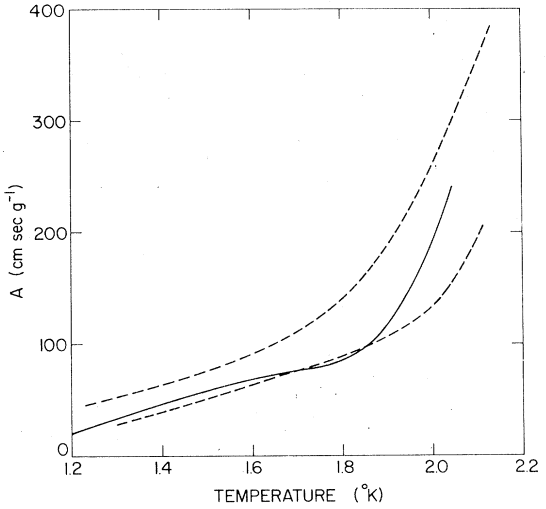

FIG. 17. Predicted and measured behavior of $A(T)$. The solid line is the theoretical prediction; the dashed lines are the data of Refs. 5 and 13.

conclusion is that reasonable changes in the modeling do not spoil the approximate agreement with experiment seen in Figs. 17–19.

It is most informative to see how the structure of λ varies with V_{ns} and T. Suppose one wishes to compute the average value of some function $f(R,\theta)$ over the distribution. Then,

$$\langle f(R,\theta)\rangle = L^{-1}\int f\left(\frac{\delta R'}{c},\theta\right) \times \lambda\left(\frac{\delta R'}{c},\theta\right)\frac{\delta^3}{c^3}R'^2\,dR'\,d\Omega\,, \qquad (53)$$

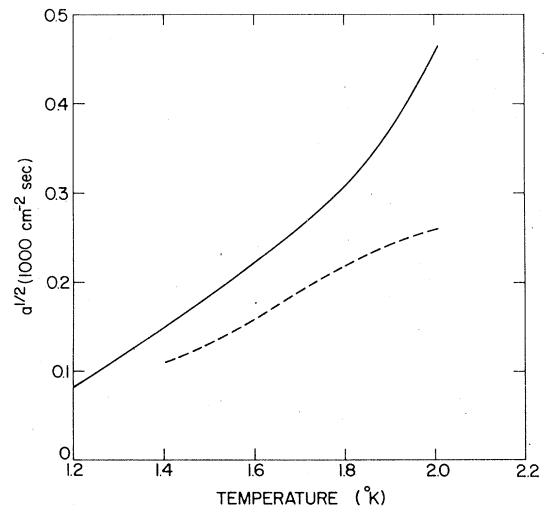

FIG. 18. Predicted and measured behavior of $a^{1/2}(T)$. The solid line is the theoretical prediction, the dashed line shows the data of Ref. 5.

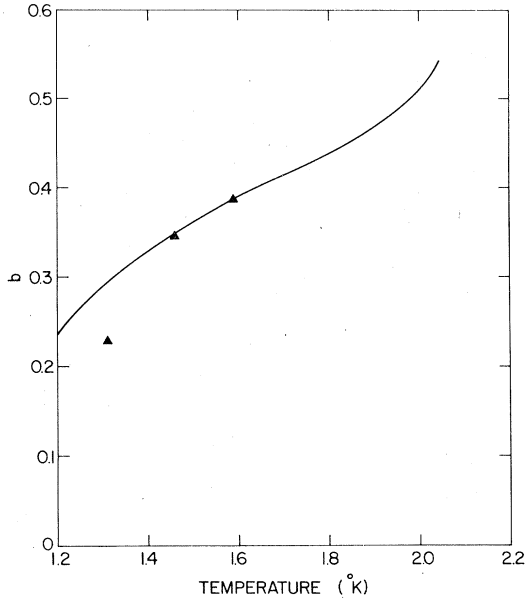

FIG. 19. Predicted and measured values of $b(T)$. The solid line is the theoretical prediction; the points are from Ref. 12.

where we have made a change of variables to $R' = cR/\delta$ in the integral. From inspection of the computed λ's, *we find that* $L^{-1}\lambda(\delta R'/c,\theta)\delta^3/c^3$ *is approximately a universal function of* R', *provided* c *is allowed to vary with temperature in the proper way*. Let us consider R_{peak}, the position of the maximum in λR^2, which can be approximately

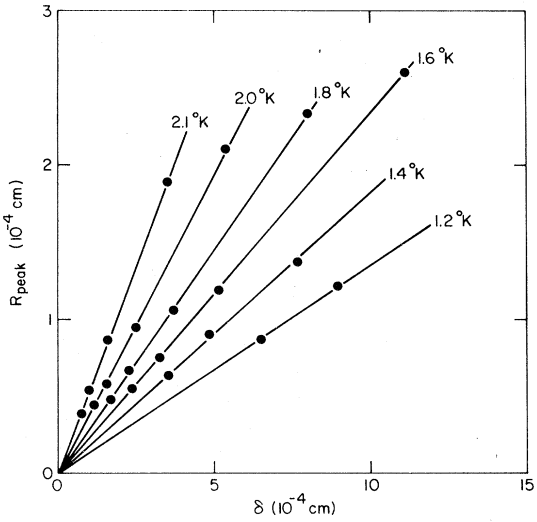

FIG. 20. Linear relation between R_{peak} and $\delta = L^{-1/2}$, indicative of the radial scaling discussed in the text. The points are the computed values, the lines are straight-line fits.

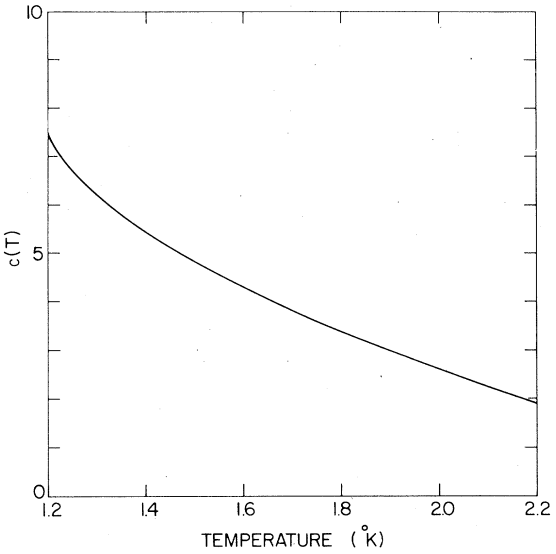

FIG. 21. Computed values of $c(T) = \delta/R_{peak}$.

identified as the characteristic radius of curvature of the tangle. The first corollary of the universality is then that $R_{peak} = \delta/c(T)$, where $c(T)$ has now been chosen such that $R'_{peak} = 1$. Figure 20 shows that indeed R_{peak} is exactly proportional to δ at any given temperature. The proportionality constant $c(T)$ can be determined from the slopes of these curves and is given in Fig. 21 for later reference. The universality also implies that

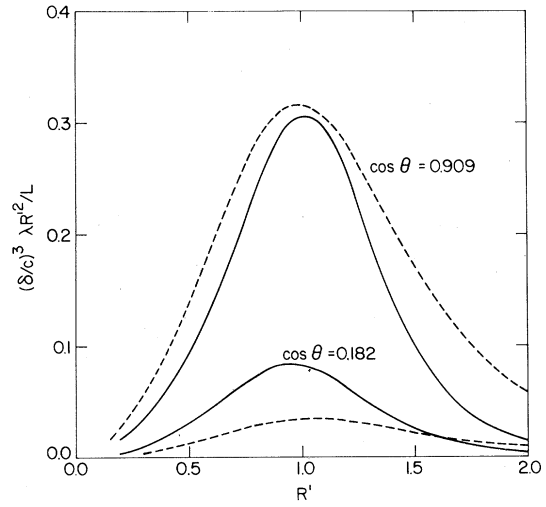

FIG. 22. Illustration of the scaling found to be a property of the steady-state λ's. The reduced λ's are plotted for the two very different cases $T = 2.0$ °K, $V_{ns} = 20$ cm sec^{-1} (dashed curves) and $T = 1.2$ °K, $V_{ns} = 5$ cm sec^{-1} (solid curves). The actual magnitudes of the unreduced distributions λR^2 differ by a factor of order 10^4 for these two cases.

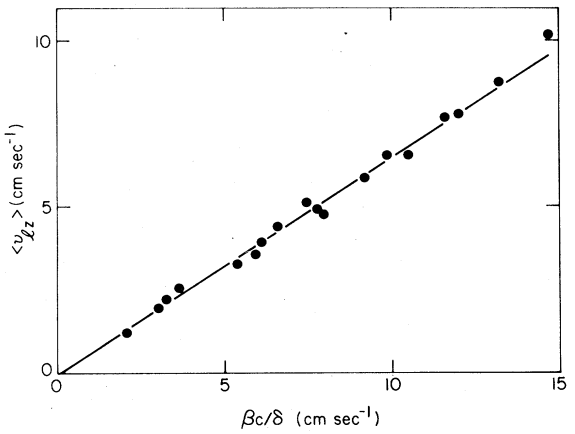

FIG. 23. Test of the universal relation $\langle v_{lz} \rangle = \text{const}\,\beta c/\delta$. The computed $\langle v_{lz} \rangle$ values from Fig. 16 are plotted here as points. The straight line corresponds to a proportionality constant equal to 0.65.

the angular variation of λ at a given R' is the same under all conditions. Figure 22 shows that this becomes more approximate at larger θ, but of course the region $\theta \sim 0$ dominates the integral of Eq. (53). As a concrete illustration of the effect of universality on a quantity depending on θ, one may consider the average drift velocity $\langle v_{lz} \rangle$ which is evaluated from Eq. (53) by using $f(R, \theta) = \beta \cos\theta/R$. The immediate implication then is that $\langle v_{lz} \rangle = \text{const.}\beta c(T)/\delta$. This relationship is certainly well obeyed (Fig. 23), demonstrating that variations in $\langle v_{lz} \rangle$ arise entirely from variations in the radial scale of λ.

A final point to be considered is the question of self-consistency; i.e., whether the condition $\langle s'' \rangle \sim \delta^{-1}$ is in fact a property of the computed solutions. Since $\langle s'' \rangle \approx R_{peak}^{-1}$, this condition is equivalent to $c(T) \sim 1$. While c does not turn out as close to 1 as one might have hoped, the order-of-magnitude consistency is reasonable. Further efforts to improve the self-consistency of the theory would probably be of value.

V. THE VINEN EQUATION

It was mentioned in Sec. I that the simple phenomenological equation developed by Vinen to fit his data has been used to analyze a number of subsequent experiments. The present work shows that the standard interpretation of this equation is, in part, incorrect. Furthermore, it is clear that some of the phenomena to which Eq. (8) has been uncritically applied really require a deeper study of the type we have attempted here. Nevertheless, an equation on the simple level of Eq. (8), properly interpreted and with its limitations kept firmly in mind, can obviously be useful. We

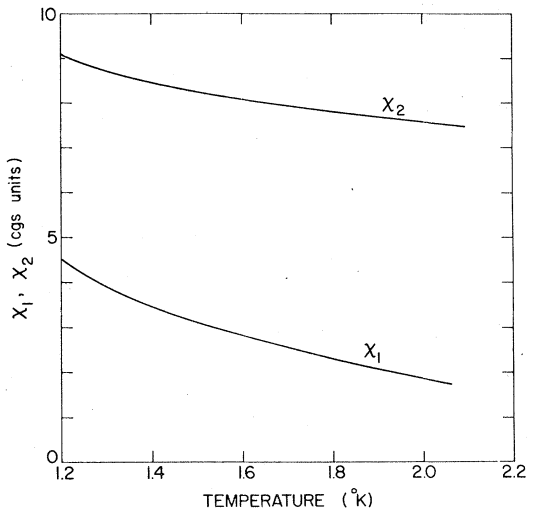

FIG. 24. Predicted values of the Vinen parameters.

now show that such an equation can indeed be obtained, and that it does in fact take the form proposed by Vinen.

To obtain the desired equation, we simply integrate Eq. (52) over R, θ space, and use the scaling properties of λ discussed in the previous section.[32] The V_{ns} terms in Eq. (35) then yield a quantity $\alpha V_{ns} c \delta^{-1} g_1 L$, and the β term gives $-\alpha\beta c^2 \delta^{-2} g_2 L$. The terms $\dot{\lambda}_3$, $\dot{\lambda}_{4,d}$, and $\dot{\lambda}_{4,k}$ make no direct contribution to $\dot{L}$, since they merely describe the redistribution of line length in R, θ space. Since $\delta = L^{-1/2}$, the integral over Eq. (52) then becomes

$$\dot{L} = \alpha c g_1 V_{ns} L^{3/2} - \alpha\beta c^2 g_2 L^2 , \tag{54}$$

where the g's are constants of order 1, and $c(T)$ has been given in Fig. 21. This result is identical to Vinen's equation, provided

$$\chi_1 = c g_1 , \quad \chi_2 (\kappa/2\pi) = \alpha\beta c^2 g_2 . \tag{55}$$

The derivation of Eq. (54) is exact within the limits of the approximate scaling behavior predicted by our theory. *The physical interpretation, however, is radically different from that originally proposed by Vinen.* Both the creation and the annihilation terms are due entirely to the action of the nonconservative forces, which cause λ to increase in one part of R, θ space and to decrease in another. The system reaches a steady state when λ has adjusted itself to the point where these competing effects balance.

It should be emphasized that the derivation of Eq. (54) was based on a property of the computed *steady-state* distributions, and does not necessarily apply when the system is far from the steady state. Equation (54) should therefore not be used to describe time-dependent properties unless there is reason to believe that the system always remains near one of its steady states. Indeed, the results shown in Figs. 11 and 12 raise the possibility that the transient behavior far from the steady state may turn out to have rather unusual properties.

The coefficients g_1 and g_2 can be evaluated from any of the steady state distributions. As expected, they are roughly independent of V_{ns} and T, g_1 varying from 0.62 to 0.72 and g_2 varying from 1.6 to 1.0 as the conditions are varied from $T = 1.2\,^{\circ}\mathrm{K}$, $V_{ns} = 5\ \mathrm{cm\,sec^{-1}}$ to $T = 2.0\,^{\circ}\mathrm{K}$, $V_{ns} = 20\ \mathrm{cm\,sec^{-1}}$. $\chi_1(T)$ and $\chi_2(T)$ take the values shown in Fig. 24. Again, the quantitative accuracy of these predictions should not be taken too seriously. Even allowing for this, however, the predicted values of the Vinen parameters differ considerably from those in the literature. At present this does not seem to present a major difficulty, since the claims of various authors to have measured these coefficients separately are all open to question. The quantity which *has* been measured with reasonable reliability is $L^{1/2}/V_{ns} = (2\pi\alpha/\kappa)(\chi_1/\chi_2)$, and this has already been displayed in Fig. 15. Further experimental studies to determine the magnitudes of χ_1 and χ_2 separately would obviously be of great interest.

VI. CONCLUSION

The physical insights provided by our model are not in disharmony with the received wisdom on the subject. The possibility that the vortex-tangle structure might be subject to some kind of scaling was first raised by Vinen.[5] Ashton and Northby[12] have modeled the turbulent state as a gas of vortex rings with $R \sim \delta$ and with v_l polarized in the direction of V_{ns}. The present work, however, goes far beyond such earlier conjectures in that it presents a coherent picture of the nature and development of the turbulent state. The approximate universality of the vortex-tangle structure, the phenomenological equation of Vinen, and the notion that most of the line has $R \sim \delta$ and v_l polarized in the direction of V_{ns} are all *consequences* of the theory.

In addition to clarifying the relevance of some of the earlier ideas about the subject, our work raises a number of qualitatively new issues. Most important among these are (a) that the self-induced motion of the line and not the random interline velocity dominates the dynamics of the tangle; (b) that *both* the creation and the annihilation of line length arises from the nonconservative interaction with the normal fluid; and (c) that line-line crossings are probably the dom-

inant mechanism which keeps the tangle random.

Finally, our theory, which contains no adjustable parameters, quantitatively predicts all of the experimentally well-established gross properties of the fully developed turbulent state. One may hope that this initial success will stimulate further experimental and theoretical work on this interesting problem.

---

[1]D. F. Brewer and D. O. Edwards, Proc. R. Soc. A 251, 247 (1959).

[2]See the review article by J. S. Langer and J. D. Reppy, in *Progress in Low Temperature Physics*, edited by C. J. Gorter (North-Holland, Amsterdam, 1970), Vol. 6, p. 1.

[3]C. J. Gorter and J. H. Mellink, Physica (Utr.) 15, 127 (1949).

[4]We follow the usual convention of letting $\vec{F}_{sn}$ denote the force exerted by the superfluid on the normal fluid.

[5]W. F. Vinen, Proc. R. Soc. A 240, 114, 128 (1957); 242, 493 (1957); 243, 400 (1958).

[6]Given the very approximate way in which Vinen was able to interpret his data, the close agreement between A and A' that he obtains is almost certainly fortuitous.

[7]D. F. Brewer and D. O. Edwards, Philos. Mag. 6, 1173 (1961).

[8]R. K. Childers and J. T. Tough, Phys. Rev. Lett. 35, 527 (1975); Phys. Rev. B 13, 1040 (1976).

[9]H. Hoch, L. Busse, and F. Moss, Phys. Rev. Lett. 34, 384 (1975); J. Mantese, G. Bischoff, and F. Moss, *ibid*. 39, 565 (1977).

[10]D. M. Sitton and F. Moss, Phys. Rev. Lett. 29, 542 (1972).

[11]R. A. Ashton and J. A. Northby, Phys. Rev. Lett. 30, 1119 (1973).

[12]R. A. Ashton and J. A. Northby, Phys. Rev. Lett. 35, 1714 (1975); R. A. Ashton, thesis (University of Rhode Island, 1977) (unpublished).

[13]D. F. Brewer and D. O. Edwards, Philos. Mag. 7, 721 (1962).

[14]H. C. Kramers, T. M. Wiarda, and A. B. Van Groenou, *Proceedings of the Seventh International Conference on Low-Temperature Physics*, edited by G. Graham and A. C. Hollis-Hallett (Univ. of Toronto, Toronto, 1961).

[15]G. Van der Heijden, W. J. P. de Voogt, and H. C. Kramers, Physica (Utr.) 59, 473 (1972).

[16]G. Van der Heijden, J. J. Giezen, and H. C. Kramers, Physica (Utr.) 61, 566 (1972).

[17]G. Van der Heijden, A. G. M. van der Boog, and H. C. Kramers, Physica (Utr.) 77, 487 (1974).

[18]R. P. Feynman, in Ref. 2, Vol. 1, p. 36.

[19]R. K. Childers and J. T. Tough, Phys. Rev. Lett. 31, 911 (1973).

[20]K. W. Schwarz, Phys. Rev. Lett. 38, 551 (1977).

[21]F. R. Hama, Phys. Fluids 6, 526 (1963).

[22]R. J. Arms and F. R. Hama, Phys. Fluids 8, 553 (1965).

[23]Throughout our discussion, β will be treated as effectively a constant.

[24]H. E. Hall and W. F. Vinen, Proc. R. Soc. A 238, 215 (1956).

[25]E. R. Huggins, Phys. Rev. A 1, 327 (1970).

[26]P. Lucas, J. Phys. C 3, 1180 (1970).

[27]In the remainder of this paper we shall use δ and $L^{-1/2}$ interchangeably.

[28]K. W. Schwarz (unpublished).

[29]It should be noted that a rather large range of ξ, corresponding to $R_{max}/R_{min} \sim 500$, was necessary to achieve this covergence.

[30]I am indebted to Dr. W. Liniger for bringing this method to my attention. Relevant references include: V. K. Saul'yev, *Integration of Equations of Parabolic Type by the Method of Nets* (Pergamon, Oxford, 1964); P. Gordon, J. Soc. Ind. Appl. Math. 13, 667 (1965); A. R. Gourlay, J. Inst. Math. Its. Appl. 6, 375 (1960).

[31]That is, the roton-dragging corrections near the λ point are probably different in a vortex tangle from those which apply to a vortex array in a rotating bucket.

[32]Essentially identical results are obtained by integrating Eq. (30) over the distribution.